

Altermagnetism in 6H perovskites

Sergey V. Streltsov^{1,2} and Sang-Wook Cheong³

¹*Institute of Metal Physics, Ural Branch of the Russian Academy of Sciences, Ekaterinburg 620137, Russia*

²*Department of theoretical physics and applied mathematics,
Ural Federal University, Ekaterinburg 620002, Russia*

³*Keck Center for Quantum Magnetism and Department of Physics and Astronomy,
Rutgers University, Piscataway, NJ 08854, USA*

(Dated: August 1, 2025)

The combination of a centrosymmetric crystallographic structure with local structural alternations and collinear antiferromagnetism can lead to broken PT (Parity \times Time-reversal) symmetry, resulting in altermagnets with non-relativistic spin-split bands. The 6H perovskites with composition $A_3BB'_2O_9$ exhibit unique layered structural alternations and typically adopt an antiferromagnetic ground state. Here, we report the discovery that several 6H perovskites are indeed altermagnets exhibiting non-relativistic spin-split bands. We also explore the possible presence of net magnetization due to spin-orbit coupling in these materials, as well as the manifestation of giant piezomagnetism. Since the single crystals of 6H perovskites can be readily grown and cleavable, our findings provide a new avenue to study the cleaved atomically-flat surfaces of altermagnets with advanced experimental techniques such as spin-resolved scanning tunneling microscopy (STM) or spin-resolved angle-resolved photoemission spectroscopy (ARPES) to explore their spin splitting nature.

PACS numbers:

INTRODUCTION

Perovskites are one of the most studied structural classes, encompassing not only the popular perovskite solar cells and the famous cuprate superconductors but also many other materials important for various applications. In so-called cubic perovskites, such as $SrTiO_3$ or $LaMnO_3$, transition metal ions are surrounded by ligand's octahedra, forming a cubic or distorted cubic lattice where the octahedra share corners. Depending on the ionic radii of the A and B elements in the general formula ABX_3 , other types of packing can be realized[1]. In hexagonal perovskites, such as $BaNiO_3$, AX_3 layers form a hexagonal close-packed structure, and the BX_6 octahedra share faces rather than corners.

Both cubic and hexagonal perovskites demonstrate extraordinary physical properties such as magnetoresistance [2], high dielectric constant [3], unusual magnetic, charge and orbital orders [4], many of them were found to be not only ferroelectrics, but also multiferroics [5, 6], other perovskites turned out half-metals with record high Curie temperatures [7].

Very recently a new notion of altermagnetism was introduced to characterize materials, which exhibit ferromagnet behavior, but have zero net magnetization [8–13]. This class of magnetic materials demonstrate anomalous electronic and spin transport, Nernst and magneto-optical effects etc. [13–15] Different perovskites have been suggested to be altermagnets: $CaCrO_3$ [16, 17], $LaTiO_3$ [18], $HgMnO_3$ [19], $(La,Ca)MnO_3$ [20, 21] and many others.

However, the simplest ABX_3 perovskites are a tip of iceberg and progress in chemistry resulted in synthesis of mixed structures, when layers of cubic per-

ovskites are intertwined with one or few layers of hexagonal (H) perovskites. In this paper we discuss altermagnetism in these mixed perovskites, so-called 6H perovskites [1, 22, 23] with general formula $A_3BB'_2O_9$ and the unit cell (u.c.) consisting of 6 repeating layers as

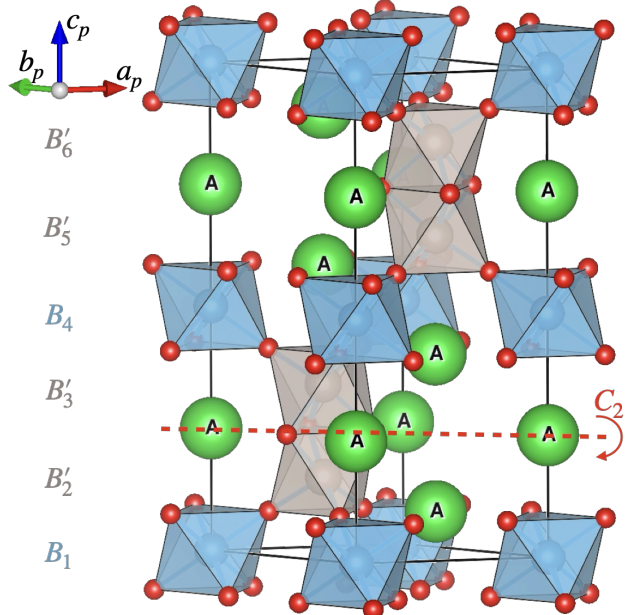


FIG. 1: The crystal structure of 6H perovskites. Magnetic ions can occupy B positions to form triangular lattice and B' constituting dimers, indexes numerate layers. For clarity a primitive unit cell (which is two times smaller than the crystallographic unit cell) is shown. The primitive c_p -axis coincides with the conventional c -axis. One of the C_2 rotation axes (at $c/4$) is sketched.

shown in Fig. 1. Magnetic ions can occupy B and B' positions, both having octahedral coordination. Two B'_2O_6 octahedra share their faces and form B'_2O_9 dimers. Both dimers and “isolated” B ions form their own triangular lattices. While the magnetic structure for most of 6H perovskites remains unsolved we argue that many of them can be altermagnets. Detailed *ab initio* calculations for two of them show not only corresponding spin-split band structure, various magneto-optical effects, but also a giant piezomagnetic response, which makes a whole class of 6H perovskite interesting for further experimental and theoretical studies.

SYMMETRY ANALYZES

There are three possible structures characterized by the hexagonal $P6_3/mmc$, orthorhombic $Cmcm$, and monoclinic $C2/c$ space groups, which describe $A_3BB'_2O_9$ perovskites with B' ions forming dimers (the hexagonal $P6_3mc$, where only half of the sites in dimers are occupied by transition metals, and the monoclinic $P2_1/c$ structures without dimers are not considered in this study) [1]. There is no inversion center (I) connecting the magnetic B sites, but C_2 rotation axes perpendicular to the c -axis (located at $1/4$ and $3/4$ of c for $Cmcm$ and $C2/c$, and additionally at the origin and $c/2$ for $P6_3/mmc$). This makes 6H perovskites altermagnetic if the two ab planes of magnetic B ions (at the origin and $c/2$) are antiferromagnetically ordered and the spins are (mostly) aligned along the c -axis. The same C_2 rotation rather than in-

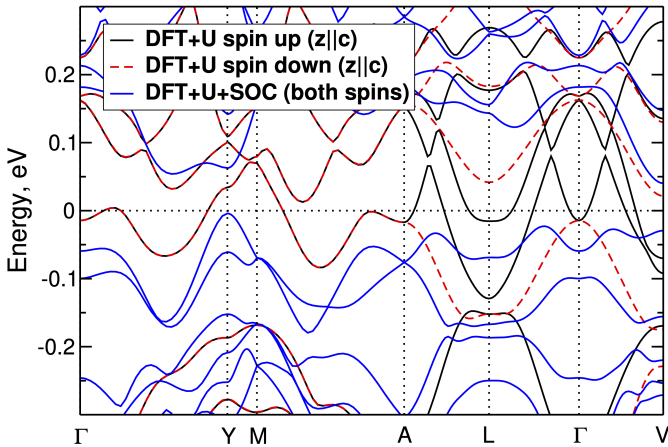


FIG. 2: The band structure of $\text{Ba}_3\text{CoIr}_2\text{O}_9$ obtained using different approximations is shown. Clear evidence for altermagnetism is observed in DFT+U calculations when moving along the $L-\Gamma-V$ direction (black and red lines); however, the material remains metallic in this approach. Including spin-orbit coupling (SOC) and a non-collinear magnetic structure leads to an insulating state (blue lines). Since SOC mixes spin up and down states, both of them are plotted for DFT+U+SOC. The Fermi energy is set to zero. High-symmetry points of the Brillouin zone are shown in Fig. 3. DFT+U+SOC band structure weighted according to different spin projections is also presented in Fig. S2 of Supplemental Materials.

version transforms B' sites of *the same* dimer into each other.

While there are many 6H perovskites with magnetic ions occupying B or B' sites, and many of them show clear signatures of dominating antiferromagnetic (AFM) interactions, a detailed study of the ground-state magnetic structure has been performed for only 15 AFM 6H perovskites. Detailed lists of ferromagnetic, ferrimagnetic, antiferromagnetic 6H perovskites, as well as those that do not exhibit long-range magnetic order being potential candidates for quantum spin-liquid behaviour or showing thermal induced magnetization, are presented in Tables S1-S3 of the supplemental materials [27].

Symmetry analysis by magnetic point groups (MPG) according to [30] shows that 4 out of 15 AFM 6H perovskites appear to be altermagnets. Their properties are summarized in Tab. I. There are two M-type altermagnets, $\text{Ba}_3\text{CoIr}_2\text{O}_9$ and $\text{Ba}_3\text{SrIr}_2\text{O}_9$, with broken time-reversal symmetry, where one would expect non-vanishing magnetization due to orbital magnetism (spin-orbit coupling). In addition, time-reversal symmetry is broken in $\text{Ba}_3\text{NiRu}_2\text{O}_9$ and $\text{Ba}_3\text{TbRu}_2\text{O}_9$, which must be S-type altermagnets with symmetric non-relativistic spin splitting. Next, we use density functional theory (DFT) calculations to verify these conclusions and study the implications of altermagnetism in one representative from each class.

DFT RESULTS

M-type altermagnet: $\text{Ba}_3\text{CoIr}_2\text{O}_9$. In M-type altermagnets, one would expect a spontaneous Hall effect if they were metallic. However, a general feature of stoichiometric 6H perovskites is that they are typically insulators. Transition metal ions occupying B sites (in the case of $\text{Ba}_3\text{CoIr}_2\text{O}_9$, these are Co^{2+} , $3d^7$) are far apart

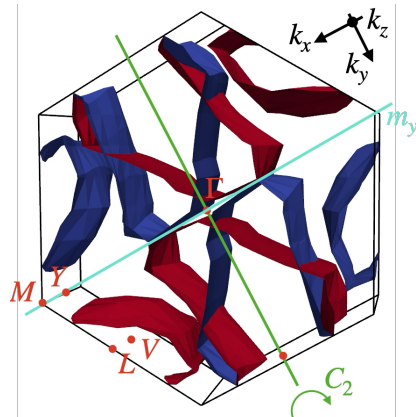


FIG. 3: The Fermi surface obtained in DFT+U calculations for $\text{Ba}_3\text{CoIr}_2\text{O}_9$ is shown. Different spin projections are indicated by blue and red. The C_2 rotation transforms all spin-up states into spin-down sheets. High-symmetry points of the Brillouin zone are marked in red (the A -point, located above the Γ -point, is not shown). m_y is the mirror plane.

Compound	Magnetic ions	T_N	Magnetic point group	Magnetic structure	Altermagnetism type	Hall	Reference
$\text{Ba}_3\text{CoIr}_2\text{O}_9$	$\text{Co}^{2+}(d^7)$, $\text{Ir}^{5+}(d^4)$	107 K	$2/m$	$\approx c$	M-type	ρ_{xz}	[14, 24]
$\text{Ba}_3\text{SrIr}_2\text{O}_9^*$	$\text{Ir}^{5+}(d^4)$	-	$2'/m'$	coll. in ac	M-type	ρ_{xy}, ρ_{yz}	[25]
$\text{Ba}_3\text{NiRu}_2\text{O}_9$	$\text{Ni}^{2+}(d^8)$, $\text{Ru}^{5+}(d^3)$	5 K	$6'/m'mm'$	$ c$	S-type	no	[14, 26, 27]
$\text{Ba}_3\text{TbRu}_2\text{O}_9$	$\text{Tb}^{4+}(f^7)$, $\text{Ru}^{4+}(d^4)$	9.5 K	$6'/m'mm'$	$ c$	S-type	no	[28, 29]

TABLE I: Altermagnets with 6H perovskite structure. Classification of altermagnetism type is according to [30]. For $\text{Ba}_3\text{SrIr}_2\text{O}_9$ the theoretical magnetic ground state obtained in previous DFT+U+SOC calculations were used for analysis; moments are collinear in the ac plane with large ferromagnetic component.

and do not share common ligands. This results in small bandwidths, which can hardly compete with a substantial Hubbard U . The B' sites (Ir^{5+} , $5d^4$) form dimers with corresponding molecular orbitals, and some electrons are delocalized over the dimer [4]. However, since the dimers are also isolated, this does not lead to metallic conductivity.

However, our situation is even more complicated. $\text{Ba}_3\text{CoIr}_2\text{O}_9$ turns out to be metallic in DFT+U calculations, as shown in Fig. 2. The band structure clearly demonstrates strong non-relativistic spin-splitting along the $L-\Gamma-V$ path, confirming the symmetry analysis. Indeed, the points Y , M , and A all belong to the m_y mirror plane (which is perpendicular to k_y). Therefore, these points are transformed only by the C_2 rotation (about the k_y axis) and inversion I . If we first apply the C_2 rotation, we change $k_x \rightarrow -k_x$, $k_z \rightarrow -k_z$, and $S_z \rightarrow -S_z$. Then, the consecutive application of I transforms these points back to their initial positions but with a flipped spin (since inversion does not affect the spin). Thus, there must be spin degeneracy: $\varepsilon(\vec{k}\uparrow) = \varepsilon(\vec{k}\downarrow)$ for any k -point belonging to the m_y mirror plane, including Y , M , and A . There is no such restriction for the L and V points (m_y is active for them and additionally flips the spin, leading only to the trivial condition $\varepsilon(\vec{k}\uparrow) = \varepsilon(\vec{k}\uparrow)$).

The altermagnetism also manifests itself in the Fermi surface (see Fig. 3), where sheets corresponding to different spins are transformed into each other by the C_2 rotation discussed in the previous section.

The spin-orbit coupling strongly changes the electronic structure of $\text{Ba}_3\text{CoIr}_2\text{O}_9$ and leads to the opening of the 40 meV band gap (blue lines in Fig. 2) [24]. Therefore, $\text{Ba}_3\text{CoIr}_2\text{O}_9$ can be classified as a spin-orbit-assisted Mott insulator [4] with zero Hall conductivity. Note, that even if U_{Co} and U_{Ir} are increased up to unrealistic 10 eV and 3 eV, respectively, this material remains metallic in DFT+U. The spin-orbit coupling is essential for the insulating ground state. The magnetic symmetry should affect not only static properties but also frequency-dependent (optical) conductivity, $\sigma_{ij}(\omega)$, which is more relevant for insulators. For the $2/m$ MPG, there can be a single off-diagonal matrix element, $\sigma_{xz}(\omega)$ (and $\sigma_{zx} = -\sigma_{xz}$). Results of direct $\sigma_{ij}(\omega)$ calculations using the Green-Kubo formalism [31] within the DFT+U+SOC approach for the experimental magnetic structure, presented in Fig. 4, confirm that this is indeed

the case.

One can probe the same physics by the magneto-optic Kerr effect (MOKE) experiments. Symmetry consideration shows that there must be 8 non-zero elements in q_{ijk} tensor relating components of the magnetic field H_k with dielectric permeability tensor $\beta_{ij} = q_{ijk}H_k$: q_{xxy} , q_{yyy} , q_{zzy} , q_{yzx} , q_{yzz} , q_{xzy} , q_{xyx} , q_{xyz} .

The M-type of altermagnetism implies weak ferromagnetism via the canting of magnetic moments. The presence of heavy Ir^{5+} ions with a large spin-orbit coupling constant and Co^{2+} ions, which are prone to having large

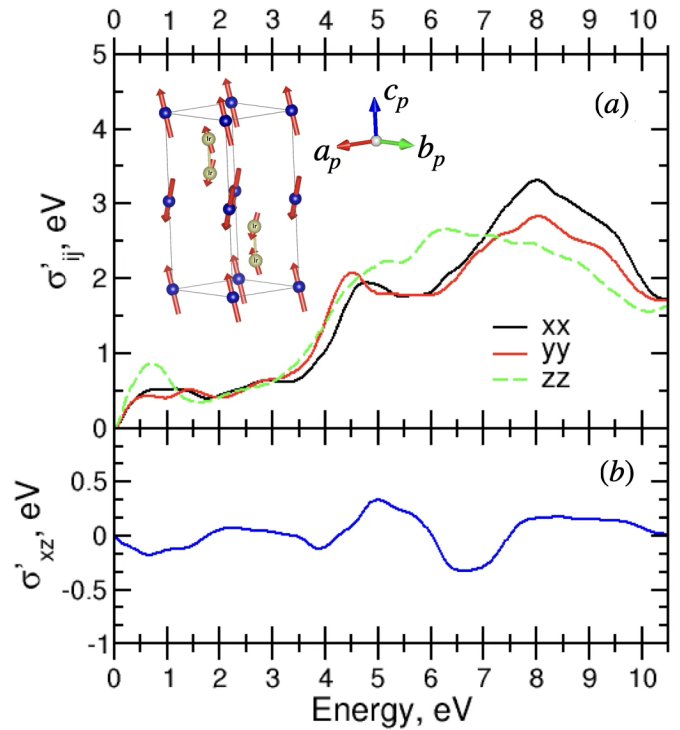


FIG. 4: The real part of the optical conductivity for $\text{Ba}_3\text{CoIr}_2\text{O}_9$, as obtained in DFT+U+SOC calculations, is shown. (a) shows three (symmetry independent) diagonal components, while (b) presents its single non-zero off-diagonal element, which serves as direct evidence of a magneto-optical effect. The magnetic configuration obtained in DFT+U+SOC calculations is presented in inset (Co is in blue, Ir is in grey), index p indicates that the primitive cell is shown.

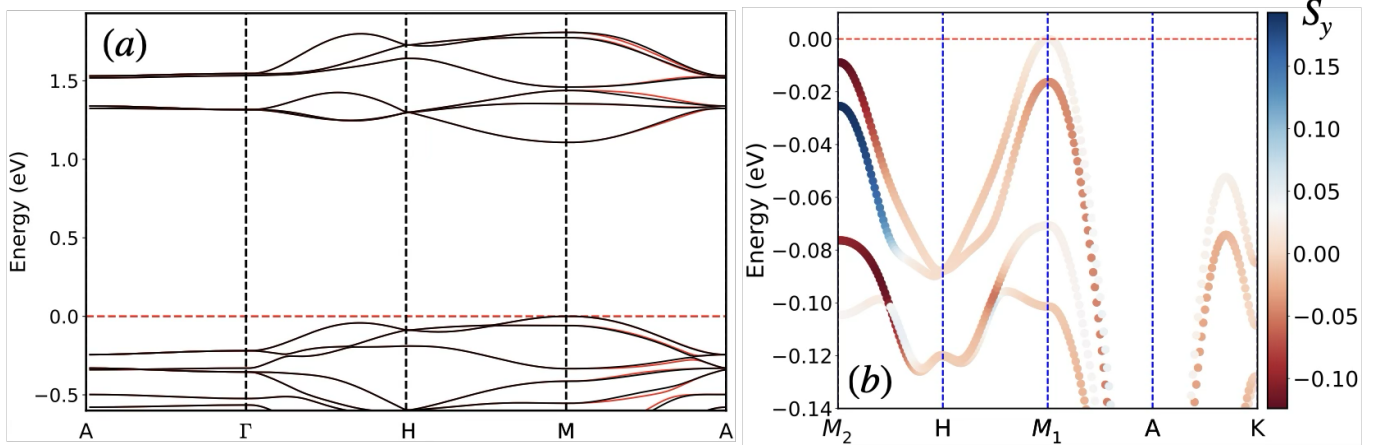


FIG. 5: Band structure of $\text{Ba}_3\text{NiRu}_2\text{O}_9$ obtained in (a) collinear AFM DFT+U calculations for experimental crystal structure (different spin projections are shown by color) and (b) in non-collinear DFT+U+SOC calculations with 1% tensile strain applied along y direction. In (b) color is used to show S_y of corresponding state. Strain makes M -points inequivalent. M_1 , M_2 , and K points are shown in inset of Fig. 6(a), while A and H are located above Γ and K points, respectively. The Fermi energy is in zero in both plots.

orbital moments, supports this tendency. This is exactly what is observed in $\text{Ba}_3\text{CoIr}_2\text{O}_9$ in DFT+U+SOC calculations. The resulting magnetic structure, respecting the C_2 rotation axes, is shown in the inset of Fig. 4(a). A net ferromagnetic moment of $1.4 \mu_B$ per formula unit (f.u.) is directed approximately along y . The canting of magnetic moments exceeds 20° on Co and 25° on Ir, which has a larger spin-orbit coupling. The x and y components of magnetic moments on different Co atoms are nearly the same by absolute values, but x component alternates (according to $2/m$ MPG) and does not contribute to the net magnetization. Situation with Ir moments is the same. Isolated Ir^{5+} ($5d^4$) ions tend to be non-magnetic $J = 0$, since orbital and spin moments cancel each other, see e.g. [4]. The non-zero magnetic moment on Ir^{5+} ($5d^4$) is related to strong distortions of the IrO_6 octahedra [32] and formation of molecular orbitals in Ir-Ir dimers [33].

S-type altermagnet: $\text{Ba}_3\text{NiRu}_2\text{O}_9$. In contrast to the previously discussed M-type altermagnetism, the magnetic structure in this case is collinear, and altermagnetism manifests itself through spin splitting along certain high-symmetry directions in the electronic band structure. Fig. 5(a) illustrates $\varepsilon(\vec{k})$ and one can readily observe such splitting along the M - A direction. There can be no linear Hall effect (magneto-optics) in S-type altermagnets, but one would expect a piezomagnetic effect.

The direct piezomagnetic effect results in onset of magnetization $m_i = \Lambda_{ijk}\sigma_{jk}$ as a response to stress given by σ_{jk} tensor (i, j, k are Cartesian coordinates). There is only one non-zero parameter of the piezomagnetic tensor Λ_{ijk} : $\Lambda_{112} = \Lambda_{211} = -2\Lambda$, $\Lambda_{222} = \Lambda$ for $6'/m'mm'$ MPG of $\text{Ba}_3\text{NiRu}_2\text{O}_9$. This means that distortion in the x direction can generate transverse magnetization (here and below we have in mind the total magnetization per u.c.) along y (Λ_{211}), strain along y can result in non-zero m_y

(Λ_{222}), while other components must vanish (for comparison, one might expect the longitudinal effect: $\sigma_{xx} \rightarrow m_x$, $\sigma_{yy} \rightarrow m_y$, and $\sigma_{zz} \rightarrow m_z$ in $\text{Ba}_3\text{CoIr}_2\text{O}_9$).

Naively, one would expect that the antisymmetric Dzyaloshinskii-Moriya interaction (activated by the lowering of symmetry from $P6_3/mmc$ to $Cmcm$ due to strain) can result in canting of the magnetic moments and the formation of a net ferromagnetic moment. However, direct DFT+U+SOC calculations, taking into account both possible non-collinearity and spin-orbit coupling, show a vanishingly small net magnetization of $\sim 10^{-3} \mu_B/2$ f.u., even when 1% strain along the y -axis is applied. This can be attributed to a weaker exchange interaction; the Néel temperature in $\text{Ba}_3\text{NiRu}_2\text{O}_9$ is two orders of magnitude lower than in $\text{Ba}_3\text{CoIr}_2\text{O}_9$, despite their similar ground-state magnetic configurations (see Table I and the insets to Figs. 4 and 6).

Analysis of the strain effect on the electronic structure reveals two significant outcomes. First, it lifts the degeneracy for some of the k -points; for example, $M_1 = (1/2, 0, 0)$ and $M_2 = (0, 1/2, 0)$ become inequivalent, as shown in Fig. 5(b). Second, there is a splitting of bands with different spin characters. Consequently, doping $\text{Ba}_3\text{NiRu}_2\text{O}_9$ by holes is expected to result in an imbalance in the spin projections, leading to the formation of a net magnetization. This is precisely what direct DFT+U+SOC calculations demonstrate.

In Fig. 6(a), the dependence of the net magnetization along the y -axis on hole doping, n_h , at a fixed tensile strain of 1% along the y -axis is shown. It should be noted that the doping leaves the total (per u.c.) m_x and m_z components vanishing, exactly following the symmetry prescriptions. Moreover, the hole doping dependence can be rationalized at a qualitative level if the band structure is colored according to spin projections.

In right inset of Fig. 6(a) the top of valence band (for

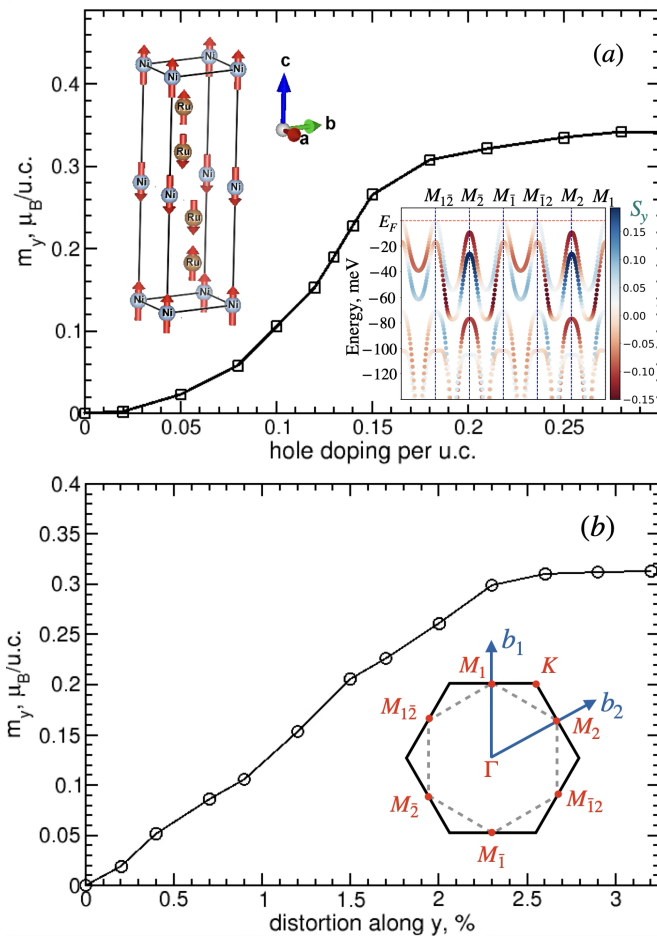


FIG. 6: Illustration of the piezomagnetic effect. (a): dependence of magnetization on doping in $\text{Ba}_{3-\delta}\text{NiRu}_2\text{O}_9$ as obtained in DFT+U+SOC calculations with 1% tensile strain along y direction applied. (b): magnetization as a function of distortion for hole doping 0.1 per unit cell (u.c.). Insets show: (a) left: experimental magnetic structure in u.c. containing 2 formula units (4 Ru and 2 Ni ions), the c -axis is along z ; right: DFT+U+SOC band structure colored according to S_y (for 1% tensile strain). (b) $q_z = 0$ cross-section of the Brillouin zone.

1% strain) is plotted if one goes along path including all M-points (their positions in Brillouin zone are shown in the top inset). Gradual doping increase up to 0.02 holes per u.c. practically does not change m_y , since electronic bands have small and nearly symmetric projections of positive and negative S_y . Corresponding depopulation of states close to $M_{1\bar{2}}, M_{\bar{1}}, M_{\bar{1}2}$, and M_1 points results in small S_y . Further doping shifts the Fermi level on more than 10 meV and to start depopulate states in M_2 and $M_{\bar{2}}$ points with much larger by absolute value S_y . As a result magnetization along y grows rapidly. Increasing doping further on we finally reach bands lying deeper in energy with opposite sign of S_y and $m_y(n_h)$ saturates. The same band structure is symmetric with respect to S_x , as shown in Fig. S1 in the supplemental materials [27]. This explains why m_x remains vanishing.

Doping can be achieved through small Ba non-stoichiometry. For instance, with $\delta = 0.1$ in $\text{Ba}_{3-\delta}\text{NiRu}_2\text{O}_9$, we obtain 0.2 holes per formula unit, or $n_h = 0.4$ holes per u.c. However, experimentally, it is more practical to apply external strain. The corresponding variation of induced magnetization is shown in Fig. 6(b) for a doping level of $n_h = 0.1$ holes per u.c. ($\delta = 0.05$).

There are two antiferromagnetic sub-lattices (Ni and Ru) in $\text{Ba}_3\text{NiRu}_2\text{O}_9$, and it is interesting to study which one contributes the most to the emerging magnetization. For example, at a doping level corresponding to 0.35 holes per u.c., each Ru ion contributes $0.1 \mu_B$ to m_y (i.e., $0.4 \mu_B/\text{u.c.}$), while Ni induces a small correction in the opposite direction, $-0.03 \mu_B$. This result is consistent with the band structure of $\text{Ba}_3\text{NiRu}_2\text{O}_9$: the Ru t_{2g} states form the top of the valence band, and the spin splitting discussed above occurs precisely in these bands. Moreover, the AFM Ru dimers are isolated in the structure of 6H perovskites, and the corresponding d bands are relatively flat. As a result, the effect of spin splitting is pronounced, leading to a large piezomagnetic effect. Additionally, Ru $^{5+}$ ions with a t_{2g}^3 electronic configuration have the maximal spin moment $S = 3/2$ (the large $t_{2g}-e_g$ crystal-field splitting in 4d transition metals breaks Hund's rules, resulting in a situation where the t_{2g} sub-shell is completely occupied first; see, e.g., [34]).

DISCUSSION AND CONCLUSIONS

Altermagnetism is closely related to the crystal structure of 6H perovskites, which lack an inversion center but possess C_2 rotation axes that transform magnetic ions in different B' planes into one another. Another crucial aspect is the nature of the exchange interaction. The BO_6 and $\text{B}'\text{O}_6$ octahedra share a common corner, and the $\angle \text{B}-\text{O}-\text{B}'$ is close to 180° , as shown in Fig. 7(a). In this configuration, the exchange interaction between the e_g orbitals is expected to be the strongest [4]. The B' sites are occupied by 4d and 5d elements, which typically adopt a low-

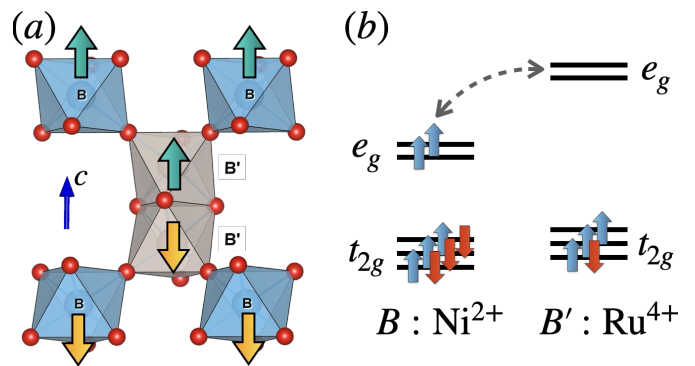


FIG. 7: Sketches illustrating origin of antiferromagnetic interplane order for B ions, due to ferromagnetic $B - B'$ and antiferromagnetic intradimer $B' - B'$ interactions (on example of Ni^{2+} and Ru^{4+} ions).

spin configuration with empty e_g orbitals. The exchange interaction between empty and half-filled e_g orbitals must be ferromagnetic, as illustrated in Fig. 7(b). This is precisely the case in both $\text{Ba}_3\text{NiRu}_2\text{O}_9$ and $\text{Ba}_3\text{CoIr}_2\text{O}_9$: the $3d$ metals occupying B sites order ferromagnetically with respect to its nearest-neighbor $4d/5d$ elements and, more importantly, this results in ferromagnetism in the ab planes, as shown in the insets of Figs. 4(a) and 6(a). The exchange interaction between the t_{2g} orbitals in B' dimers with a common face tends to be antiferromagnetic, which, together with the ferromagnetic B - B' exchange, ultimately results in antiferromagnetic order between the two (ferromagnetic) B' planes and altermagnetism, when we take into account the structural features of 6H perovskites (i.e., the C_2 axes).

If a non-magnetic ion such as Sb^{5+} or Nb^{5+} is placed into the B' sites, the in-plane magnetic order between the $3d$ metals switches to antiferromagnetic. These materials either form a 120° antiferromagnetic structure or have been suggested to exhibit spin-liquid behavior, as shown in Tables S1 and S3. In the ordered case, where the magnetic unit cell is larger than the crystallographic unit cell, these materials cannot formally be considered altermagnets. However, they might possess a ferromagnetic point group. Examples include $\text{Ba}_3\text{CoSb}_2\text{O}_9$ with the $\bar{6}m2$ MPG, $\text{Ba}_3\text{MnNb}_2\text{O}_9$ with the $3m$ MPG, and $\text{Ba}_3\text{MnSb}_2\text{O}_9$ with the 2 MPG. This “quasialtermagnetism” with $\vec{Q} \neq 0$ is likely related to magneto-elastic interactions and is expected to be weaker than in conventional altermagnets. Nevertheless, these materials could still be of significant interest due to their potential for non-trivial magneto-optical or piezomagnetic responses, as well as other effects dictated by symmetry.

Thus, 6H perovskites based on $3d$ and $4d/5d$ magnetic ions represent a promising combination of crystal structure and exchange interactions for realizing altermagnetism. Through direct ab *initio* calculations, we not only demonstrate that they are indeed altermagnets but also reveal giant piezomagnetism in $\text{Ba}_3\text{NiRu}_2\text{O}_9$, which is an order of magnitude larger than previously expected [35]. Further studies of other mixed perovskites with 4H, 9R, and other layer sequences may uncover additional altermagnets with extraordinary physical properties.

METHODS

DFT calculations were performed by the Vienna ab initio simulation package (VASP)[36]. The Perdew-Burke-Ernzerhof version of exchange correlation potential was used [37]. The crystal structures were taken from Refs. [26] and [38]. Strong Coulomb correlations were treated by DFT+U approach[39] with $U_{\text{Ni}} = 8$ eV,

$U_{\text{Co}} = 7$ eV, $U_{\text{Ru}} = 3$ eV, $U_{\text{Ir}} = 1.5$ eV, $J_{\text{Ni}} = J_{\text{Co}} = 1$ eV, $J_{\text{Ru}} = 0.7$ eV and $J_{\text{Ir}} = 0.5$ eV, close to typical values previously used for transition metal oxides [40–43]. For both materials experimental magnetic structure was used [26, 38]. The $6 \times 6 \times 4$ mesh in the Brillouin zone was utilized for self-consistent calculations (increase up to $7 \times 7 \times 5$ k-points did not change the results). The calculations were performed using the tetrahedron method with Blöchl corrections, except for magneto-optics, where the Gaussian broadening [44] of 50 meV was chosen (complex shift in the Kramers-Kronig transformation was set to 100 meV in this case). The convergence criteria for electronic iterations was set to 2×10^{-7} eV. For piezomagnetic effect calculations the spin-orbit coupling was taken into account. We used experimental crystal structure in these calculations, strains were introduced via modification of the unit cell, atomic positions were not relaxed.

DATA AVAILABILITY

All data generated or analyzed during this study are available from the corresponding authors upon reasonable request.

ACKNOWLEDGMENTS

S.V.S. would like to thank M. Braden, V. Mineev for stimulating discussions and A. Gubkin for helping with symmetry analysis.

The first-principle calculations were supported by the Russian Science Foundation via project RSF 23-12-00159, while symmetry analysis was performed with support by Ministry of Science and Higher Education of the Russian Federation. S.-W.C. was supported by the W. M. Keck foundation grant to the Keck Center for Quantum Magnetism at Rutgers University.

AUTHOR CONTRIBUTIONS

S.-W.C. and S.V.S. conceived the project. S.V.S. performed DFT calculations and symmetry analysis. S.-W.C. and S.V.S. discussed all results. S.V.S. wrote the paper.

COMPETING INTERESTS

The authors declare no competing interests.

ADDITIONAL INFORMATION

Supplementary information The online version contains supplementary material available at to-be-add-by-publisher.

Correspondence and requests for materials should be addressed to S. V. Streltsov.

¹ De, S. *et al.* Chemistry and physics of triple perovskite oxides: A topical review. *Chemistry of Materials* **36**, 9207–

9233 (2024).

² Kobayashi, K.-I., Kimura, T., Sawada, H., Terakura, K. &

- Tokura, Y. Room-temperature magnetoresistance in an oxide material with an ordered double-perovskite structure. *Nature* **395**, 677–680 (1998).
- ³ Merz, W. J. The electric and optical behavior of BaTiO₃ single-domain crystals. *Physical Review* **76**, 1221 (1949).
- ⁴ Streltsov, S. & Khomskii, D. Orbital physics in transition metal compounds: New trends. *Physics-Uspenki* **60**, 1121 (2017).
- ⁵ Cheong, S.-W. & Mostovoy, M. Multiferroics: a magnetic twist for ferroelectricity. *Nature Materials* **6**, 13–20 (2007).
- ⁶ Khomskii, D. Classifying multiferroics: Mechanisms and effects. *Physics* **2**, 20 (2009).
- ⁷ Liu, Z. *et al.* Realization of a half metal with a record-high curie temperature in perovskite oxides. *Advanced Materials* **34**, 2200626 (2022).
- ⁸ Noda, Y., Ohno, K. & Nakamura, S. Momentum-Dependent Band Spin Splitting in Semiconducting MnO₂: A Density Functional Calculation. *Physical Chemistry Chemical Physics* **18**, 13294–13303 (2016).
- ⁹ Hayami, S., Yanagi, Y. & Kusunose, H. Momentum-dependent spin splitting by collinear antiferromagnetic ordering. *Journal of the Physical Society of Japan* **88**, 123702 (2019).
- ¹⁰ Naka, M. *et al.* Spin current generation in organic antiferromagnets. *Nature Communications* **10** (2019).
- ¹¹ Ahn, K.-H., Hariki, A., Lee, K.-W. & Kuneš, J. Antiferromagnetism in RuO₂ as D-Wave Pomeranchuk Instability. *Physical Review B* **99** (2019).
- ¹² Yuan, L.-D., Wang, Z., Luo, J.-W., Rashba, E. I. & Zunger, A. Giant Momentum-Dependent Spin Splitting in Centrosymmetric Low-Z Antiferromagnets. *Physical Review B* **102**, 014422 (2020).
- ¹³ Šmejkal, L., Sinova, J. & Jungwirth, T. Emerging research landscape of altermagnetism. *Physical Review X* **12**, 040501 (2022).
- ¹⁴ Guo, Y. *et al.* Spin-split collinear antiferromagnets: A large-scale ab-initio study. *Materials Today Physics* **32**, 100991 (2023). 2207.07592.
- ¹⁵ Song, C. *et al.* Altermagnets as a new class of functional materials. *Nature Reviews Materials* (2025).
- ¹⁶ Naka, M., Motome, Y. & Seo, H. Perovskite as a spin current generator. *Physical Review B* **103**, 125114 (2021).
- ¹⁷ Streltsov, S., Korotin, M., Anisimov, V. & Khomskii, D. Band versus Localized Electron Magnetism in CaCrO₃. *Physical Review B* **78**, 054425 (2008).
- ¹⁸ Maznichenko, I. V. *et al.* Fragile Altermagnetism and Orbital Disorder in Mott Insulator LaTiO₃ (2024). 2411.00583.
- ¹⁹ Myakotnikov, D. A., Komleva, E. V., Long, Y. & Streltsov, S. V. Importance of the indirect exchange interaction via s states in altermagnetic HgMnO₃. *Physical Review B* **110**, 134427 (2024).
- ²⁰ Šmejkal, L., González-Hernández, R., Jungwirth, T. & Sinova, J. Crystal time-reversal symmetry breaking and spontaneous hall effect in collinear antiferromagnets. *Science Advances* **6**, eaaz8809 (2020).
- ²¹ Solovyev, I. V. Magneto-Optical Effect in the Weak Ferromagnets LaMO₃ (M= Cr, Mn, and Fe). *Physical Review B* **55**, 8060–8063 (1997).
- ²² Hinatsu, Y. Diverse structures of mixed-metal oxides containing rare earths and their magnetic properties. *Journal of the Ceramic Society of Japan* **123**, 845–852 (2015).
- ²³ Nguyen, L. T. & Cava, R. J. Hexagonal perovskites as quantum materials. *Chemical Reviews* **121**, 2935–2965 (2021).
- ²⁴ Garg, C. *et al.* Evolution of the Structural, Magnetic, and Electronic Properties of the Triple Perovskite Ba₃CoIr₂O₉. *Physical Review B* **103**, 014437 (2021).
- ²⁵ Nag, A. *et al.* Ba₃MIr₂O₉ Hexagonal Perovskites in the Light of Spin-Orbit Coupling and Local Structural Distortions. *Physical Review B* **97**, 064408 (2018).
- ²⁶ Lightfoot, P. & Battle, P. D. The Crystal and Magnetic Structures of Ba₃NiRu₂O₉, Ba₃CoRu₂O₉, and Ba₃ZnRu₂O₉. *Journal of Solid State Chemistry* **89**, 174 (1990).
- ²⁷ See Supplemental Material at URL-will-be-inserted-by-publisher.
- ²⁸ Doi, Y. *et al.* Crystal Structures and Magnetic Properties of the 6H-Perovskites Ba₃LnRu₂O₉ (Ln = Ce, Pr and Tb). *Journal of Materials Chemistry* **11**, 3135–3140 (2001).
- ²⁹ Doi, Y. *et al.* Magnetic and Calorimetric Studies on 6H-Perovskite Ba₃TbRu₂O₉. *Journal of Alloys and Compounds* **344**, 166–169 (2002).
- ³⁰ Cheong, S.-W. & Huang, F.-T. Altermagnetism classification. *npj Quantum Materials* **10**, 38 (2025).
- ³¹ Gajdoš, M., Hummer, K., Kresse, G., Furthmüller, J. & Bechstedt, F. Linear optical properties in the projector-augmented wave methodology. *Physical Review B* **73**, 045112 (2006).
- ³² Nag, A. *et al.* Origin of the Spin-Orbital Liquid State in a Nearly J=0 Iridate Ba₃ZnIr₂O₉. *Phys. Rev. Lett.* **116**, 097205 (2016).
- ³³ Streltsov, S. & Khomskii, D. Orbital-dependent singlet dimers and orbital-selective peierls transitions in transition-metal compounds. *Physical Review B* **89**, 161112 (2014).
- ³⁴ Khomskii, D. I. & Streltsov, S. V. Magnetic oxides. In *Encyclopedia of Condensed Matter Physics*, 98–111 (Elsevier, 2024).
- ³⁵ Ma, H.-Y. *et al.* Multifunctional antiferromagnetic materials with giant piezomagnetism and noncollinear spin current. *Nature Communications* **12**, 2846 (2021).
- ³⁶ Kresse, G. & Furthmüller, J. Efficient iterative schemes for ab initio total-energy calculations using a plane-wave basis set. *Phys. Rev. B* **54**, 11169 (1996).
- ³⁷ Perdew, J. P., Burke, K. & Ernzerhof, M. Generalized gradient approximation made simple. *Phys. Rev. Lett.* **78**, 1396(E) (1997).
- ³⁸ Doi, Y., Hinatsu, Y. & Ohoyama, K. Structural and Magnetic Properties of Pseudo-Two-Dimensional Triangular Antiferromagnets Ba₃MSb₂O₉ (M = Mn, Co, and Ni). *Journal of Physics: Condensed Matter* **16**, 8923–8935 (2004).
- ³⁹ Dudarev, S. L., Savrasov, S. Y., Humphreys, C. J. & Sutton, A. P. Electron-Energy-Loss Spectra and the Structural Stability of Nickel Oxide: An LSDA+U Study. *Physical Review B* **57**, 1505–1509 (1998).
- ⁴⁰ Streltsov, S. Magnetic Moment Suppression in Ba₃CoRu₂O₉: Hybridization Effect. *Physical Review B* **88**, 024429 (2013).
- ⁴¹ Muthuselvam, I. *et al.* Two-Step Antiferromagnetic Transition and Moderate Triangular Frustration in Li₂Co(WO₄)₂. *Physical Review B* **90**, 174430 (2014).
- ⁴² Terzic, J. *et al.* Coexisting Charge and Magnetic Orders in the Dimer-Chain Iridate Ba₅AlIr₂O₁₁. *Physical Review B* **91**, 235147 (2015).
- ⁴³ Zvereva, E. *et al.* Orbitally Induced Hierarchy of Exchange Interactions in the Zigzag Antiferromagnetic State of Hon-

- eycomb Silver Delafossite Ag₃Co₂SbO₆. *Dalton Transactions* **45** (2016).
- ⁴⁴ Methfessel, M. & Paxton, A. T. High-precision sampling for brillouin-zone integration in metals. *Physical Review B* **40**, 3616–3621 (1989).